CHEMISTRY
A European Journal

A Journal of
ChemPubSoc Europe

Accepted Article

Title: Efficient Fused Ring Extension of A-D-A-type Nonfullerene Acceptors via Symmetric Replicating Core Unit Strategy

Authors: Yanming Sun, Tian Xia, Chao Li, Hwa Sook Ryu, Jing Guo, Jie Min, and Han Young Woo

To be cited as: *Chem. Eur. J.* 10.1002/chem.202000889

Link to VoR: http://dx.doi.org/10.1002/chem.202000889

Supported by
ACES

WILEY-VCH

10.1002/chem.202000889

RESEARCH ARTICLE

WILEY-VCH

Efficient Fused Ring Extension of A-D-A-type Nonfullerene Acceptors via Symmetric Replicating Core Unit Strategy

Tian Xia[+], Chao Li[+], Hwa Sook Ryu, Jing Guo, Jie Min, Han Young Woo, and Yanming Sun*

Abstract: Extension of a fused aromatic ring core is beneficial for enhancing the intramolecular charge transfer and effective π-conjugation in A-D-A type non-fullerene acceptors (NFAs). In this work, a novel strategy involving extension of fused-ring core by symmetrically replicating core unit was developed, and a novel symmetric fused-12-ring NFA, LC81 was synthesized. When paired with the wide-bandgap polymer donor, PBT1-C, the corresponding organic solar cells (OSCs) showed a high-power conversion efficiency (PCE) of 12.71%, much higher than that of the device based on reference NFA, TPTT-4F. Moreover, the LC81-based OSC displayed a lower energy loss and a better ambient stability than the TPTT-4F-based device. Our results indicate that the extension of fused-ring core by symmetric replicating core unit is an effective strategy for promoting photovoltaic characteristics of A-D-A-type NFAs.

Introduction

Bulk-heterojunction (BHJ) organic solar cells (OSCs), composed of an electron donor and an electron acceptor, have received significant attention due to their light-weight, semitransparency, mechanical flexibility and compatibility with roll-to-roll large-area printing manufacturing.[1-4] Recently, non-fullerene acceptors (NFAs) have successfully replaced fullerene and its derivatives in OSCs, owing to their unique advantages of easily tunable molecular energy levels and broad light absorption ranges well as good photostability and thermal stability.[5-9] Since the fused-ring electron acceptor, ITIC, with an acceptor-donor-acceptor (A-D-A) configuration reported by Zhan and co-workers in 2015,[10] A-D-A-type NFAs have experienced rapid developments,[8-31] and OSCs based on such A-D-A-type NFAs have surpassed 16% power conversion efficiencies (PCEs).[32-34] As it is well known that, in A-D-A-type NFAs, such A-D-A backbone structures are conducive to modulating the intramolecular charge transfer (ICT) and π-conjugation. With respect to the D unit, the indacenodithiophene (IDT) unit with five-membered fused rings possesses a sufficiently rigid coplanar architecture, which has been extensively employed to design high-performance A-D-A-type NFAs. In order to further investigate the ICT effect for the IDT based A-D-A-type NFAs, various approaches have been developed to modify the chemical structure of IDT central core, and much effort has been focused on introducing more fused rings to extend the π-conjugation.[13-17, 20, 35]

In this regard, there are mainly two strategies for fused ring extension of IDT core unit (Figure 1).[36, 37] The most common way is the symmetric fused ring extension on both sides of the IDT, attaining symmetric A-D-A-type NFAs.[38-41] For example, Zhan and co-workers have designed and synthesized a series of NFAs named F7IC, F9IC, and F11IC,[38] which all possess symmetric extension of fused-rings at thiophene positions of both side of the IDT unit. Through this strategy, the frontier molecular orbital (FMO) energy levels and band gap could be fine-tuned, and the molecular packing and electron mobility were significantly improved, leading to enhanced open-circuit voltage (V_{oc}), short-circuit current density (J_{sc}), and fill factor (*FF*) of OSCs, simultaneously. On the other hand, to precisely tune the energy levels, absorption, and the molecular packing of the molecules, another strategy emerged, which involves an asymmetric fused ring extension on each side of the IDT unit, thus obtaining asymmetric A-D-A-type NFAs.[14, 15, 17, 40] For instance, the asymmetric A-D-A-type NFA, TPTT-2F and TPTTT-2F reported by our group were acquired by fusing one thiophene or thieno[3,2-b]thiophene on only one side of symmetric IDT (TPT), respectively. Moreover, we developed an NFA, TTPTTT-4F, which also possessed asymmetric fused ring extension, and the corresponding OSC yielded a PCE of up to 12.05%. In addition to the fine regulating, the larger dipole moment may also facilitate molecular interaction for such asymmetric NFAs to promote photovoltaic performance. However, how to reduce the energy loss (E_{loss}) to further improve the PCE for OSCs remains a key challenge in material design. Intriguingly, in 2016, Liao et al. reported a multiply fused-ring NFA IDTIDT-IC of which D unit consists of two IDT units fused together, thus bearing a fused 10-heterocyclic ring with extended π-conjugated system.[42] Although the IDTIDT-IC-based device yielded a moderate PCE of 6.5% when PTB7-Th was used as donor material, this OSC presented an E_{loss} as low as 0.59 eV and a relatively high V_{oc} of 0.94 V. Despite scarce similar studies on it, this work has provided us with great inspiration into molecular design.

Herein, we demonstrate a new strategy named symmetric replicating core unit strategy, that is the extension of fused-ring core by symmetrically replicating D unit and fusing them together (Figure 1). The resulting new core unit may exhibit prominently extended π-conjugated system and enhanced electron-donating ability, which is conducive to stronger ICT and higher lowest unoccupied molecular orbital (LUMO) energy level for the NFA, thus leading to higher V_{oc} and low E_{loss} once blended with donor

T. Xia,[+] C. Li,[+] Prof. Y. Sun
School of Chemistry, Beihang University
Beijing 100191 (P. R. China)
E-mail: sunym@buaa.edu.cn

H. S. Ryu, Prof. H. Y. Woo
Department of Chemistry, College of Science
Korea University
Seoul 136–713, Republic of Korea

J. Guo, Prof. J. Min
The Institute for Advanced Studies, Wuhan University, Wuhan 430072;
Key Laboratory of Materials Processing and Mold (Zhengzhou University),
Ministry of Education, Zhengzhou, 450002 (P. R. China)

[+] These authors contributed equally to this work.

Supporting information for this article is given via a link at the end of the document.

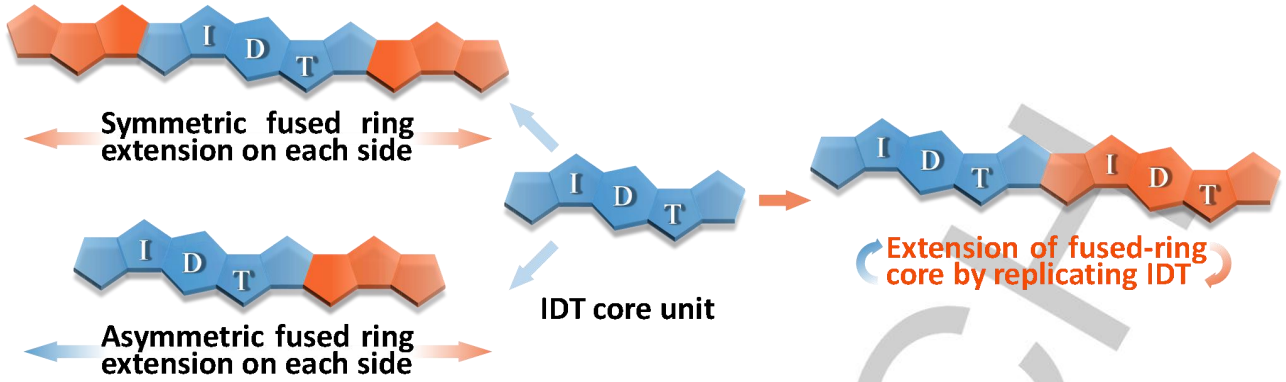

Figure 1. Three fused-ring core extension strategies for IDT based A-D-A-type NFAs.

materials in OSCs. This is very essential for the future development of high-performance OSCs, whereas less research has focused on it. Therefore, the development and understanding of symmetric replicating core unit strategy is extremely challenging and important.

In this contribution, we chose an asymmetric TPTT unit developed by our group as the parent D unit to design and synthesize the novel 12-membered IDT derivative core unit and its corresponding symmetric A-D-A-type NFA LC81 *via* a symmetric replication of TPTT unit to extend the fused-ring core (Figure 2). LC81 and reference material TPTT-4F shared the same difluorinated 1,1-dicyanomethylene-3-indanone (IC) end-capping group, while the symmetric LC81 was found to present redshifted absorption, upshifted FMO energy levels and higher electron mobility compared with TPTT-4F. When paired with the wide-bandgap polymer donor PBT1-C, the LC81-based blend film presented more balanced charge transport, more efficient exciton dissociation and reduced bimolecular recombination relative to the TPTT-4F-based blend film. As a consequence, the OSCs based on PBT1-C:LC81 showed a maximum PCE of up to 12.71% with a V_{oc} of 0.875 V, a J_{sc} of 19.84 mA cm^{-2}, and a *FF* of 73.2%, which are all higher than those of the PBT1-C:TPTT-4F devices. Moreover, the LC81-based OSCs displayed a lower E_{loss} and a better ambient stability than the TPTT-4F-based devices. Our results demonstrated that the extension of fused-ring core by symmetric replicating core unit strategy to obtain efficient symmetric core with extended π-conjugation is an effective way for promoting photovoltaic performances of A-D-A-type NFAs-based OSCs.

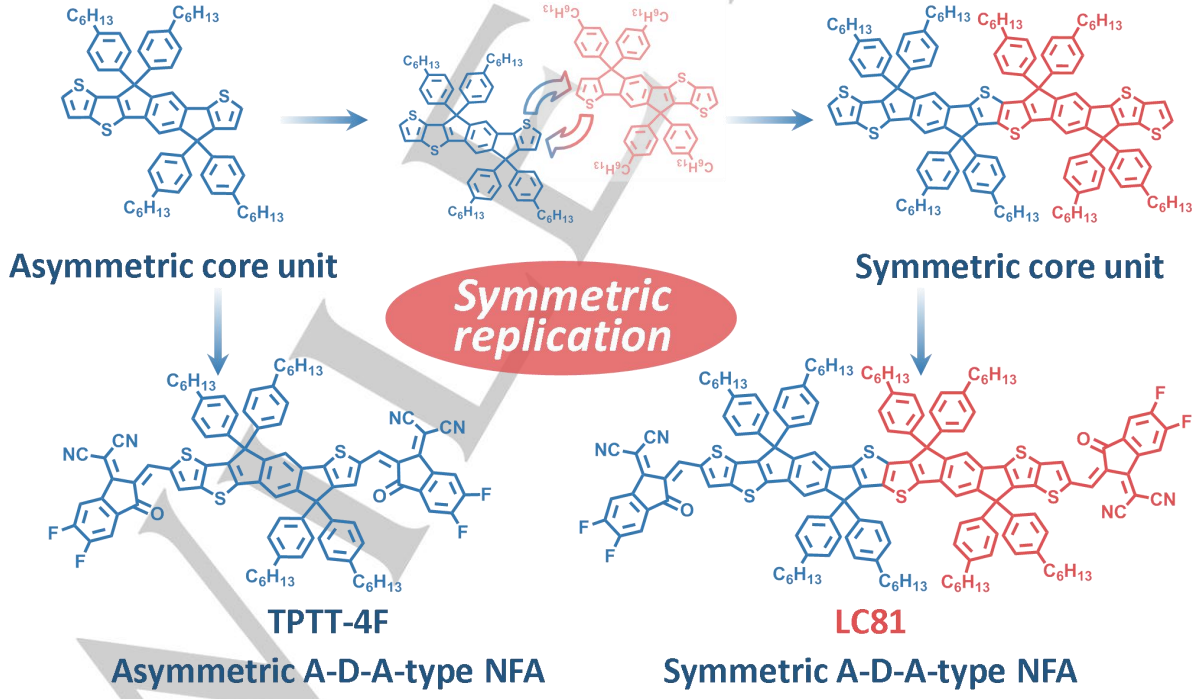

Figure 2. Molecular design strategy and chemical structures of TPTT-4F and LC81.

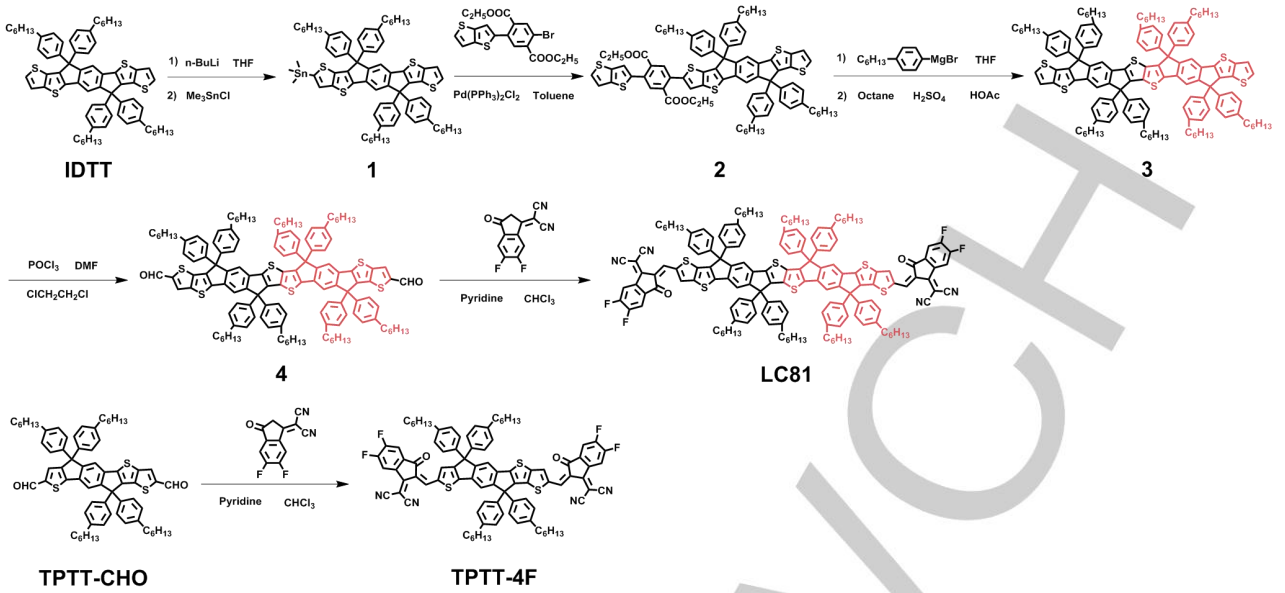

Scheme 1. Synthetic routes to LC81 and TPTT-4F.

Results and Discussion

The synthetic routes toward LC81 and TPTT-4F were presented in Scheme **1**. Starting with the commercially available IDTT, the monolithiation of IDTT and the subsequent addition of trimethyltin chloride afforded compound **1**, which was directly reacted with diethyl 2-bromo-5-(thieno[3,2-b]thiophen-2-yl)terephthalate through Stille coupling reaction to give compound **2**. The treatment of compound **2** with the fleshly prepared 4-octylbenzene magnesium bromide yielded diol, which was then subjected to intramolecular Friedel-Crafts cyclization to furnish compound **3**. This compound 3 was reacted with $POCl_3$ and DMF to yield compound **4**, which was further reacted with 2-(5,6-difluoro-3-oxo-2,3-dihydro-1H-inden-1-ylidene)malononitrile by Knoevenagel condensation reaction to afford a desirable compound LC81. The Knoevenagel condensation reaction between TPTT-CHO and 2-(5,6-difluoro-3-oxo-2,3-dihydro-1H-inden-1-ylidene)malononitrile yielded TPTT-4F. All the new compounds were characterized by ^{1}H NMR, ^{13}C NMR, and MS (MALDI-TOF). Both TPTT-4F and LC81 showed good solubility in common solvents like dichloromethane, chloroform, and chlorobenzene at room temperature.

The normalized UV-vis absorption spectra of TPTT-4F and LC81 in dilute chloroform solution and thin films are shown in Figure 3a and 3b, and the corresponding data are summarized in Table 1. In solution, LC81 exhibits maximum absorption peak at 730 nm, which shows a 50 nm red shift relative to that of TPTT-4F, because of its enhanced electron-donating ability and conjugation length of the fused-ring core. From the solution to the film, a red-shifted maximum absorption and broader spectrum can be observed for both NFAs, relative to their corresponding solution spectra. The maximum absorption peak of TPTT-4F and LC81 were red-shifted from 680 nm to 724 nm and from 730 to 754 nm, respectively, indicating more intensive π-π cofacial intermolecular interactions in the solid state for both NFAs. The thin film absorption onset of LC81 extended to over 850 nm, corresponding to an optical bandgap (E_g^{opt}) of 1.45 eV, which is decreased by ~0.12 eV with respect to that of TPTT-4F.

The electrochemical characteristics of these two NFAs were studied through cyclic voltammetry (CV), and the corresponding oxidation and reduction curves are shown in Figure 3c. The onset oxidation/reduction potentials of TPTT-4F and LC81 were measured to be 1.37/-0.29 and 1.12/-0.40 V vs. Ag/Ag^+, respectively. Thus, the corresponding highest occupied molecular orbital (HOMO)/ LUMO energy levels of TPTT-4F and LC81 were then determined to be -5.74/-4.08 and -5.49/-3.97 eV, respectively. These results implied that by symmetric replication core unit strategy, the novel central core unit with more extended π-conjugation can upshift HOMO and LUMO levels of LC81 simultaneously, with compared to TPTT-4F. Noteworthily, as a result of the extended core unit with a stronger ICT effect in LC81 compared to TPTT-4F, LC81 showed a higher LUMO level, which contributed to achieving a higher V_{oc} in OSC devices. Interestingly, the elevation in the HOMO energy level of LC81 was more pronounced than that of the LUMO energy level, and the HOMO offset between LC81 and the polymer donor PBT1-C is lower than 0.01 eV. The corresponding electrochemical data are listed in Table 1.

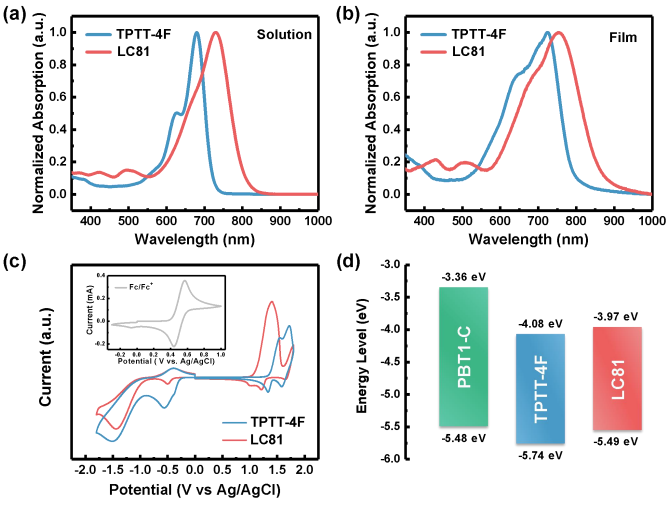

Figure 3. Normalized absorption spectra of TPTT-4F and LC81 in (a) chloroform solution and (b) thin films. (c) Cyclic voltammograms of TPTT-4F and LC81. (d) Energy level diagram of PBT1-C, TPTT-4F and LC81.

Table 1. Optical and electrochemical data of TPTT-4F and LC81.

NFA	λ_{max} [nm][a]	λ_{max} [nm][b]	λ_{onset} [nm][b]	E_g^{opt} [eV][c]	E_{ox} [V]	HOMO [eV]	E_{red} [V]	LUMO [eV]
TPTT-4F	680	724	789	1.57	1.37	-5.74	-0.29	-4.08
LC81	730	754	858	1.45	1.12	-5.49	-0.40	-3.97

[a] In $CHCl_3$ solution. [b] In thin film drop cast from $CHCl_3$ solution. [c] Estimated from empirical formula: $E_g^{opt} = 1240/\lambda_{onset}$.

To probe photovoltaic properties of these two NFAs, the OSCs were fabricated with an inverted device structure of indium tin oxide (ITO)/ZnO/PBT1-C:NFA/MoO_3/Ag, in which the PBT1-C is a wide-bandgap polymer donor. Employing chloroform as the processing solvent, the optimized PBT1-C/LC81 weight ratio was 1:1.1 (w/w) with 0.4 vol% 1,8-diiodooctane (DIO) as a processing additive. Similarly, the TPTT-4F-based OSC was also optimized with a PBT1-C/TPTT-4F weight ratio of 1:1.2(w/w), and 0.2 vol% DIO. The detailed device optimization results are provided in Figure S1-S2 and Table S1-S2, and the *J-V* curves and corresponding photovoltaic parameters of the optimized OSCs are shown in Figure 4a and Table 2. The optimal device based on PBT1-C:LC81 delivered a maximum PCE of up to 12.71%, accompanied by a V_{oc} of 0.875 V, a J_{sc} of 19.84 mA cm^{-2} and a *FF* of 73.2%, and these parameters were all superior to PBT1-C:TPTT-4F (a PCE of 10.40%, a V_{oc} of 0.795 V, a J_{sc} of 18.25 mA cm^{-2} and a *FF* of 71.7%). The higher PCE of the LC81-based device was ascribed to simultaneous increases of V_{oc}, J_{sc}, and *FF* with compared to those of the TPTT-4F-based device. The fact that the V_{oc} of LC81-based device is higher than that of TPTT-4F-based device was well consistent with the up-shifted LUMO energy level of LC81 relative to TPTT-4F. The external quantum efficiency (EQE) spectra of the optimized devices are shown in Figure 4b. Compared to the photo response of the TPTT-4F-based device in the wavelength range of 300-800 nm, the device based on LC81 exhibited a much broader photo response, extending from 300 to 900 nm. The results of the EQE agreed well with the neat film absorption profiles of these two NFAs. Therefore, the PBT1-C:LC81 based OSC device presented an impressive integrated J_{sc} of 18.93 mA cm^{-2}, which was also higher than that of the PBT1-C:TPTT-4F based device (17.41 mA cm^{-2}), even though the maximum EQE value of LC81-based device was slightly lower than that of TPTT-4F-based device. These integrated J_{sc} values were in good agreement with the J_{sc} values determined from *J-V* curves, within 5% deviation.

Device stability is also a significant parameter affecting the potential commercialization of OSCs. In consequence, the ambient stability of both two optimized OSC devices without encapsulation was tested. As depicted in Figure 4f, the optimized devices based on PBT1-C:LC81 still maintained over 80% of their initial PCE values after 800 h under ambient conditions, whereas only about 70% of the initial PCE was retained for the TPTT-4F-based

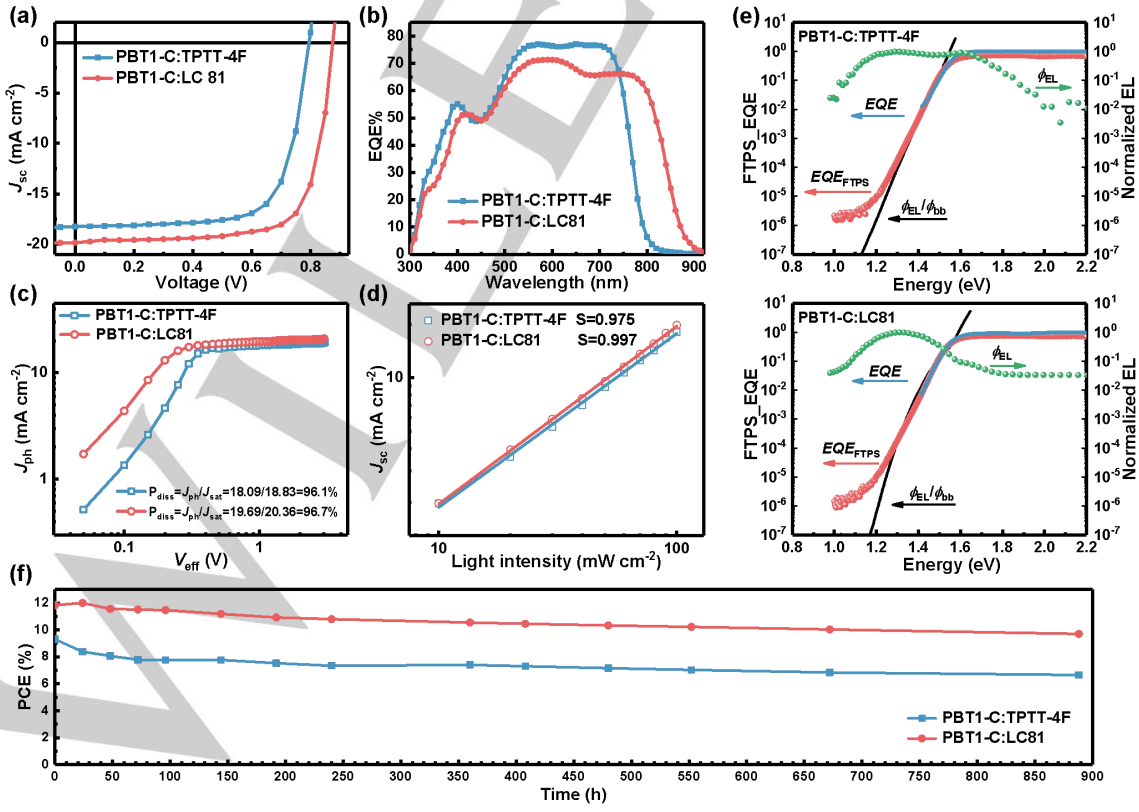

Figure 4. (a) *J-V* curves and (b) EQE curves of the optimal OSC devices based on the PBT1-C:NFA blend. (c) Measured quantum efficiency (EQE, blue line), Fourier transform photocurrent spectroscopy (FTPS-EQE, red lines), electroluminescence (EL, green lines), and external quantum efficiency (black lines) of the optimal OSC devices based on PBT1-C:TPTT-4F and PBT1-C:LC81, respectively. The evolution of (d) J_{ph} versus V_{eff} and (e) light intensity dependence of J_{sc} for the optimized OSC devices. (f) The PCEs for the unencapsulated optimal OSC devices based on PBT1-C:TPTT-4F and PBT1-C:LC81 after exposure to air for various time.

Table 2. Photovoltaic data of the optimized OSCs based on PBT1-C:NFA

NFA	V_{oc} [V][a]	J_{sc} [mA/cm^2][a]	$J_{sc,cal}$ [mA/cm^2]	*FF* [%][a]	PCE [%][a]
TPTT-4F	0.795 (0.793±0.003)	18.25 (18.15±0.04)	17.41	71.7 (70.35±1.91)	10.40 (10.13±0.33)
LC81	0.875 (0.883±0.014)	19.84 (19.63±0.21)	18.93	73.2 (72.60±0.61)	12.71 (12.58±0.12)

[a] Average values with standard deviations were obtained from 20 devices.

device, in the same environment. These results suggest that through symmetric replication core unit strategy, the π-conjugated system of the fused-ring core for the NFA could be prominently extended, which is beneficial to improve the photovoltaic performance and ambient stability of the corresponding OSC devices.

To quantify the charge transport properties of the these two NFA-based neat films and the corresponding blend films, the space-charge-limited current (SCLC) were measured. It was found that the LC81-based neat film possessed an average electron mobility (μ_e) of 6.99×10^{-4} cm^{2}V^{-1}s^{-1}, which is relatively higher than that of the neat film based on TPTT-4F (5.85×10^{-4} cm^{2}V^{-1}s^{-1}). As for the blend films, the average hole mobilities (μ_h)/electron mobilities of PBT1-C:LC81 and PBT1-C:TPTT-4F were measured to be 12.41×10^{-4}/5.52×10^{-4} and 10.09×10^{-4}/3.75×10^{-4} cm^{2}V^{-1}s^{-1}, which corresponded to the calculated μ_h/μ_e ratios of 2.25 and 2.69, respectively. It is noteworthy that the LC81-based blend film showed promoted electron mobility and more balanced charge carrier transport relative to the TPTT-4F-based blend film, which could well explain the higher J_{sc} and *FF* values obtained in the OSCs based on PBT1-C:LC81. The related data are provided in Figure S3 and Table S3.

The exciton dissociation and charge collection characteristics were evaluated by measuring the photocurrent density (J_{ph}) versus effective voltage (V_{eff}). As shown in Figure 4c, for both two NFAs-based devices, the J_{ph} would be raised as the V_{eff} increased. The saturated J_{ph} (J_{sat}) values were obtained when the V_{eff} was greater than 2 V, suggesting that all photogenerated excitons were dissociated into free charge carriers and collected by electrodes. The J_{sat} value of the optimal device based on PBT1-C:LC81 was measured to be 20.36 mA cm^{-2}, which is approximately 8% higher than that of optimized TPTT-4F-based device (18.83 mA cm^{-2}), proving that the core unit with more extended π-conjugated system by symmetric replication of TPTT unit benefited the absorption spectrum broadening and charge generation, and thus promoted J_{sc}. Under the short-circuit conditions, the exciton dissociation probability (P_{diss}) could be confirmed by measuring the J_{ph}/J_{sat} ratio. The P_{diss} values of PBT1-C:LC81 and PBT1-C:TPTT-4F devices were calculated to be 96.7% and 96.1%, respectively, demonstrating that both two NFAs-based OSCs possessed efficient exciton dissociation and charge collection efficiency.

To further understand the charge recombination behaviors in both two NFAs-based OSC devices, the corresponding J_{sc} versus light intensity (P_{light}) curves were measured. The relationship between the J_{sc} and P_{light} could be interpreted based on the formula, $J_{sc} \propto P_{light}^{S}$, in which the exponential factor *s* denotes the degree of bimolecular recombination. If the value of *s* is equal to 1, it means that all free charges are swept out and collected by the electrodes prior to recombination, while $s < 1$ indicates there is some degree of bimolecular recombination.[43-46] As Figure 4d depicted, the *s* value of the PBT1-C:LC81-based device was calculated to be 0.997, which was slightly higher than that of TPTT-4F-based device (0.975). These data implied that a much weaker bimolecular charge recombination occurs in optimized LC81-based OCS device relative to TPTT-4F-based device, and such negligible charge recombination facilitated higher J_{sc} and *FF* for corresponding OSCs.

Electroluminescence (EL) spectra and Fourier-transform photocurrent spectroscopy (FTPS) measurements were carried out to estimate the E_{loss} of these two photovoltaic systems (Figure 4e). Following the detailed balance theory, the E_{loss} ($q\Delta V_{oc}$) can be categorized into three different parts: $q\Delta V_{oc} = \left(E_{gap} - qV_{oc}^{SQ}\right) + q\Delta V_{oc}^{rad} + q\Delta V_{oc}^{nonrad}$.[47-50] The effective bandgap (E_{gap}) determined from the crossing point of the blended film absorption and EL spectra were 1.653 eV for PBT1-C:TTPT-4F and 1.483 eV for PBT1-C:LC81, respectively (Figure S4). The first part, $\Delta E_1 = E_{gap} - qV_{oc}^{SQ}$, depending on E_{gap} and the theoretical maximum voltage by the Shockley-Queisser limit, were 0.278 and 0.250 eV for TPTT-4F and LC81, respectively. The LC81-based device exhibited a slightly smaller ΔE_1 value, whereas this substantial loss is inevitable.[51] The second part, $\Delta E_2 = q\Delta V_{oc}^{rad}$, is the voltage loss *via* radiative recombination from the absorption below the bandgap, because of the charge transfer (CT) state in the OSCs. As show in Table 3, it was found that the LC81 system presented a negligible ΔE_2 of 0.045 eV, which was 0.15 eV lower than that of the TPTT-4F-based devices, reflecting that PBT1-C:LC81 had higher CT-state excitons.[52] The third part, $\Delta E_3 = q\Delta V_{oc}^{nonrad}$, originated from the non-radiative recombination and could be determined from the EQE of the EL measurements. The PBT1-C:LC81 device gave a relatively small $q\Delta V_{oc}^{nonrad}$ of 0.297 V, which was also nearly 0.1 eV lower in contrast to that of TPTT-4F system (0.396 eV), attributing to the effective suppression of non-radiative recombination loss in the LC81 system. In addition, the lower non-radiative recombination loss as compared to the TPTT-4F-based device can also be attributed to the lower offsets between PBT1-C and LC81, resulting in hybridization between charge-transfer and lowest donor or acceptor exciton states. As a result, the total E_{loss} of the optimized device based on PBT1-C:LC81 was determined to be 0.592 eV, which is much lower than that of TPTT-4F-based device (0.869 eV).

Table 3. Summary of Parameters Measured and Calculated from FTPS-EQE and EL

NFA	E_{gap} [eV]	V_{oc} [V]	E_{loss} [eV]	V_{oc}^{SQ} [V]	$\Delta E_1 = E_{gap} - qV_{oc}^{SQ}$ [eV]	V_{oc}^{rad} [V]	$\Delta E_2 = q\Delta V_{oc}^{rad}$ [eV]	$\Delta E_3 = q\Delta V_{oc}^{nonrad}$ [eV]
TPTT-4F	1.653	0.784	0.869	1.375	0.278	1.18	0.195	0.396
LC81	1.483	0.891	0.592	1.233	0.250	1.188	0.045	0.297

The atomic force microscopy (AFM) was employed to get a deep insight into the morphologies of these two NFA-based blend films. As displayed in Figure S5, from the AFM height images, it can be seen that the PBT1-C:LC81-based and PBT1-C:TPTT-4F-based blend films both presented smooth and uniform surfaces with relatively small root mean square (RMS) roughness of 2.03 nm and 1.03 nm, respectively. In details, the distinct fibril network morphology occurred in both blend films, as shown in the AFM phase images, which is favorable of efficient exciton dissociation and charge carriers transport.[4, 53] The molecular orientation and packing behaviors of these two A-D-A-type NFAs neat films were investigated via grazing incident wide-angle X-ray scattering (GIWAXS) measurements. The 2D GIWAXS patterns and corresponding line-cuts profiles of TPTT-4F, and LC81 neat films were displayed in Figure S6. It could be observed that TPTT-4F neat films exhibited weak lamellar and π-π stacking scatterings, demonstrating that TPTT-4F possessed relatively weak crystallinity due to the steric hindrance caused by the presence of the phenyl side chains. In the in-plane (IP) direction, the (100) lamellar stacking peak could be observed at 0.33 $Å^{-1}$ in the TPTT-4F neat film, and the corresponding lamellar stacking *d*-spacing was calculated to be 19.0 Å. As for the LC81 neat film, the appearance of (100) lamellar stacking peak at q = 0.36 $Å^{-1}$ (*d*-spacing=17.4 Å) in the IP direction indicated relatively higher degree of crystallinity than that of TPTT-4F, which showed a good agreement with the SCLC results as mentioned above.

Conclusion

In conclusion, by symmetric replicating core unit strategy, we designed and synthesized a symmetric 12-membered IDT derivative core unit and its corresponding symmetric A-D-A-type NFA LC81. The LC81 possessed a fused-ring core with more extended π-conjugated system, and it was found to possess redshifted absorption, upshifted FMO energy levels and higher electron mobility relative to TPTT-4F. When blending with PBT1-C, the optimized OSC based on PBT1-C:LC81 delivered a superior PCE of 12.71%, which is much higher than that (10.40%) of TPTT-4F-based OSC. The simultaneous enhancements of V_{oc}, J_{sc} and FF account for the high PCE achieved in PBT1-C:LC81 OSCs. Furthermore, LC81-based devices also exhibited a lower E_{loss} and better ambient stability in contrast to TPTT-4F-based devices. Therefore, by symmetrically replicating fused-ring core unit to extend π-conjugated system is an effective strategy to promote photovoltaic performance of A-D-A-type NFAs.

Supporting information

Supporting Information is available from the Wiley Online Libraryor from the author.

Acknowledgements

This work was financially supported by the National Natural Science Foundation of China (NSFC) (Grant Nos. 21734001, 51825301, and 21674007). HYW is grateful for the financial support from the National Research Foundation (NRF) of Korea (NRF-2016M1A2A2940911, 2019R1A6A1A11044070).

Conflict of interest

The authors declare no conflict of interest.

Keywords: fused ring extension • extend π-conjugated system • indacenodithiophene • symmetric replicating core unit strategy • low energy loss

1. Y. Cai, L. Huo and Y. Sun, *Adv. Mater.*, 2017, **29**, 1605437.
2. H. Fu, Z. Wang and Y. Sun, *Angew. Chem., Int. Ed.*, 2019, **58**, 4442-4453.
3. H. Fu, Z. Wang and Y. Sun, *Sol. RRL*, 2018, **2**, 1700158.
4. T. Xia, Y. Cai, H. Fu and Y. Sun, *Sci. China: Chem.*, 2019, **62**, 662-668.
5. J. Hou, O. Inganäs, R. H. Friend and F. Gao, *Nat. Mater.*, 2018, **17**, 119-128.
6. J. Zhang, H. S. Tan, X. Guo, A. Facchetti and H. Yan, *Nat. Energy*, 2018, **3**, 720-731.
7. R. Yu, H. Yao and J. Hou, *Adv. Energy Mater.*, 2018, **8**, 1702814.
8. Y. Li, L. Zhong, J.-D. Lin, F.-P. Wu, H.-J. Bin, Z. Zhang, L. Xu, Z.-Q. Jiang, Z.-G. Zhang, F. Liu, T. P. Russell, Y. Li, L.-S. Liao and S. R. Forrest, *Sol. RRL*, 2017, **1**, 1700107.
9. B. Kan, H. Feng, H. Yao, M. Chang, X. Wan, C. Li, J. Hou and Y. Chen, *Sci. China: Chem.*, 2018, **61**, 1307-1313.
10. Y. Lin, J. Wang, Z.-G. Zhang, H. Bai, Y. Li, D. Zhu and X. Zhan, *Adv. Mater.*, 2015, **27**, 1170-1174.
11. Y. Li, D. Qian, L. Zhong, J.-D. Lin, Z.-Q. Jiang, Z.-G. Zhang, Z. Zhang, Y. Li, L.-S. Liao and F. Zhang, *Nano Energy*, 2016, **27**, 430-438.
12. F. Wu, L. Zhong, H. Hu, Y. Li, Z. Zhang, Y. Li, Z.-G. Zhang, H. Ade, Z.-Q. Jiang and L.-S. Liao, *J. Mater. Chem. A*, 2019, **7**, 4063-4071.
13. R. Ming, J. Wang, W. Gao, M. Zhang, J. Gao, W. Ning, Z. Luo, X. Liu, C. Zhong, F. Zhang and C. Yang, *Small Methods*, 2019, **3**, 1900280.
14. J. Song, C. Li, L. Ye, C. Koh, Y. Cai, D. Wei, H. Y. Woo and Y. Sun, *J. Mater. Chem. A*, 2018, **6**, 18847-18852.
15. C. Li, Y. Xie, B. Fan, G. Han, Y. Yi and Y. Sun, *J. Mater. Chem. C*, 2018, **6**, 4873-4877.
16. C. Li, J. Song, Y. Cai, G. Han, W. Zheng, Y. Yi, H. S. Ryu, H. Y. Woo and Y. Sun, *J. Energy Chem.*, 2020, **40**, 144-150.

17. C. Li, J. Song, L. Ye, C. Koh, K. Weng, H. Fu, Y. Cai, Y. Xie, D. Wei, H. Y. Woo and Y. Sun, *Sol. RRL*, 2019, **3**, 1800246.
18. C. Li, T. Xia, J. Song, H. Fu, H. S. Ryu, K. Weng, L. Ye, H. Y. Woo and Y. Sun, *J. Mater. Chem. A*, 2019, **7**, 1435-1441.
19. L. Ye, Y. Xie, Y. Xiao, J. Song, C. Li, H. Fu, K. Weng, X. Lu, S. Tan and Y. Sun, *J. Mater. Chem. A*, 2019, **7**, 8055-8060.
20. S. Li, W. Liu, C.-Z. Li, T.-K. Lau, X. Lu, M. Shi and H. Chen, *J. Mater. Chem. A*, 2016, **4**, 14983-14987.
21. D. He, F. Zhao, L. Jiang and C. Wang, *J. Mater. Chem. A*, 2018, **6**, 8839-8854.
22. B. Gao, H. Yao, J. Hou, R. Yu, L. Hong, Y. Xu and J. Hou, *J. Mater. Chem. A*, 2018, **6**, 23644-23649.
23. Y. Lin, Q. He, F. Zhao, L. Huo, J. Mai, X. Lu, C.-J. Su, T. Li, J. Wang, J. Zhu, Y. Sun, C. Wang and X. Zhan, *J. Am. Chem. Soc.*, 2016, **138**, 2973-2976.
24. H. Lin, S. Chen, Z. Li, J. Y. L. Lai, G. Yang, T. McAfee, K. Jiang, Y. Li, Y. Liu, H. Hu, J. Zhao, W. Ma, H. Ade and H. Yan, *Adv. Mater.*, 2015, **27**, 7299-7304.
25. S. Li, L. Ye, W. Zhao, S. Zhang, S. Mukherjee, H. Ade and J. Hou, *Adv. Mater.*, 2016, **28**, 9423-9429.
26. W. Zhao, S. Li, H. Yao, S. Zhang, Y. Zhang, B. Yang and J. Hou, *J. Am. Chem. Soc.*, 2017, **139**, 7148-7151.
27. S. Zhang, Y. Qin, J. Zhu and J. Hou, *Adv. Mater.*, 2018, **30**, 1800868.
28. D. Xie, T. Liu, W. Gao, C. Zhong, L. Huo, Z. Luo, K. Wu, W. Xiong, F. Liu, Y. Sun and C. Yang, *Sol. RRL*, 2017, **1**, 1700044.
29. Y. Cui, H. Yao, L. Hong, T. Zhang, Y. Xu, K. Xian, B. Gao, J. Qin, J. Zhang, Z. Wei and J. Hou, *Adv. Mater.*, 2019, **31**, 1808356.
30. T.-W. Chen, K.-L. Peng, Y.-W. Lin, Y.-J. Su, K.-J. Ma, L. Hong, C.-C. Chang, J. Hou and C.-S. Hsu, *J. Mater. Chem. A*, 2020, **8**, 1131-1137.
31. S. M. Swick, W. Zhu, M. Matta, T. J. Aldrich, A. Harbuzaru, J. T. Lopez Navarrete, R. Ponce Ortiz, K. L. Kohlstedt, G. C. Schatz, A. Facchetti, F. S. Melkonyan and T. J. Marks, *Proc. Natl. Acad. Sci. USA*, 2018, **115**, E8341.
32. Q. An, X. Ma, J. Gao and F. Zhang, *Sci. Bull.*, 2019, **64**, 504-506.
33. D. Li, X. Chen, J. Cai, W. Li, M. Chen, Y. Mao, B. Du, J. A. Smith, R. C. Kilbride, M. E. O'Kane, X. Zhang, Y. Zhuang, P. Wang, H. Wang, D. Liu, R. A. L. Jones, D. G. Lidzey and T. Wang, *Sci. China: Chem.*, 2020, DOI: 10.1007/s11426-019-9681-8.
34. J. Song, C. Li, L. Zhu, J. Guo, J. Xu, X. Zhang, K. Weng, K. Zhang, J. Min, X. Hao, Y. Zhang, F. Liu and Y. Sun, *Adv. Mater.*, 2019, **31**, 1905645.
35. S. Dai, F. Zhao, Q. Zhang, T.-K. Lau, T. Li, K. Liu, Q. Ling, C. Wang, X. Lu, W. You and X. Zhan, *J. Am. Chem. Soc.*, 2017, **139**, 1336-1343.
36. C. Li, H. Fu, T. Xia and Y. Sun, *Adv. Energy Mater.*, 2019, **9**, 1900999.
37. H. Wang, J. Cao, J. Yu, Z. Zhang, R. Geng, L. Yang and W. Tang, *J. Mater. Chem. A*, 2019, **7**, 4313-4333.
38. S. Dai, Y. Xiao, P. Xue, J. James Rech, K. Liu, Z. Li, X. Lu, W. You and X. Zhan, *Chem. Mater.*, 2018, **30**, 5390-5396.
39. B. Jia, S. Dai, Z. Ke, C. Yan, W. Ma and X. Zhan, *Chem. Mater.*, 2018, **30**, 239-245.
40. B. Jia, J. Wang, Y. Wu, M. Zhang, Y. Jiang, Z. Tang, T. P. Russell and X. Zhan, *J. Am. Chem. Soc.*, 2019, DOI: 10.1021/jacs.9b08988.
41. J. Sun, X. Ma, Z. Zhang, J. Yu, J. Zhou, X. Yin, L. Yang, R. Geng, R. Zhu, F. Zhang and W. Tang, *Adv. Mater.*, 2018, **30**, 1707150.
42. Y. Li, X. Liu, F.-P. Wu, Y. Zhou, Z.-Q. Jiang, B. Song, Y. Xia, Z.-G. Zhang, F. Gao, O. Inganäs, Y. Li and L.-S. Liao, *J. Mater. Chem. A*, 2016, **4**, 5890-5897.
43. P. Schilinsky, C. Waldauf and C. J. Brabec, *Appl. Phys. Lett.*, 2002, **81**, 3885-3887.
44. I. Riedel, N. Martin, F. Giacalone, J. L. Segura, D. Chirvase, J. Parisi and V. Dyakonov, *Thin Solid Films*, 2004, **451-452**, 43-47.
45. D. Gebeyehu, M. Pfeiffer, B. Maennig, J. Drechsel, A. Werner and K. Leo, *Thin Solid Films*, 2004, **451-452**, 29-32.
46. J. Min, Y. N. Luponosov, N. Gasparini, M. Richter, A. V. Bakirov, M. A. Shcherbina, S. N. Chvalun, L. Grodd, S. Grigorian, T. Ameri, S. A. Ponomarenko and C. J. Brabec, *Adv. Energy Mater.*, 2015, **5**, 1500386.
47. J. Benduhn, K. Tvingstedt, F. Piersimoni, S. Ullbrich, Y. Fan, M. Tropiano, K. A. McGarry, O. Zeika, M. K. Riede, C. J. Douglas, S. Barlow, S. R. Marder, D. Neher, D. Spoltore and K. Vandewal, *Nat. Energy*, 2017, **2**, 17053.
48. Y. Xie, T. Li, J. Guo, P. Bi, X. Xue, H. S. Ryu, Y. Cai, J. Min, L. Huo, X. Hao, H. Y. Woo, X. Zhan and Y. Sun, *ACS Energy Lett.*, 2019, **4**, 1196-1203.
49. X. Li, K. Weng, H. S. Ryu, J. Guo, X. Zhang, T. Xia, H. Fu, D. Wei, J. Min, Y. Zhang, H. Y. Woo and Y. Sun, *Adv. Funct. Mater.*, 2019, **n/a**, 1906809.
50. Y. Wang, D. Qian, Y. Cui, H. Zhang, J. Hou, K. Vandewal, T. Kirchartz and F. Gao, *Adv. Energy Mater.*, 2018, **8**, 1801352.
51. J. Liu, S. Chen, D. Qian, B. Gautam, G. Yang, J. Zhao, J. Bergqvist, F. Zhang, W. Ma, H. Ade, O. Inganäs, K. Gundogdu, F. Gao and H. Yan, *Nat. Energy*, 2016, **1**, 16089.
52. H. Chinese Journal of ChemistryYao, D. Qian, H. Zhang, Y. Qin, B. Xu, Y. Cui, R. Yu, F. Gao and J. Hou, *Chin. J. Chem.*, 2018, **36**, 491-494.
53. T. Liu, L. Huo, S. Chandrabose, K. Chen, G. Han, F. Qi, X. Meng, D. Xie, W. Ma, Y. Yi, J. M. Hodgkiss, F. Liu, J. Wang, C. Yang and Y. Sun, *Adv. Mater.*, 2018, **30**, 1707353.

10.1002/chem.202000889

Entry for the Table of Contents

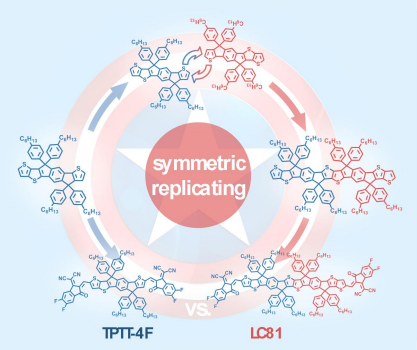

The extension of fused-ring core by symmetric replicating core unit is an effective strategy for promoting photovoltaic performance of A-D-A-type NFAs.